Wave-particle interactions in the equatorial source region of whistler-mode emissions

O. Santolík,[1,2] D. A. Gurnett,[3] J. S. Pickett,[3] S. Grimald,[4] P. M. E. Décreau,[5] M. Parrot,[5] N. Cornilleau-Wehrlin,[6,7] F. El-Lemdani Mazouz,[8] D. Schriver,[9] N. P. Meredith,[10] and A. Fazakerley[4]

[1]   Wave-particle interactions can play a key role in the process of transfer of energy between different electron populations in the outer Van Allen radiation belt. We present a case study of wave-particle interactions in the equatorial source region of whistler-mode emissions. We select measurements of the Cluster spacecraft when these emissions are observed in the form of random hiss with only occasional discrete chorus wave packets, and where the wave propagation properties are very similar to previously analyzed cases of whistler-mode chorus. We observe a positive divergence of the Poynting flux at minima of the magnetic field modulus along the magnetic field lines, indicating the central position of the source. In this region we perform a linear stability analysis based on the locally measured electron phase space densities. We find two unstable electron populations. The first of them consists of energy-dispersed and highly anisotropic injected electrons at energies of a few hundreds eV to a few keV, with the perpendicular temperature more than 10 times higher than the parallel temperature with respect to the magnetic field line. Another unstable population is formed by trapped electrons at energies above 10 keV. We show that the injected electrons at lower energies can be responsible for a part of the waves that propagate obliquely at frequencies above one half of the electron cyclotron frequency. Our model of the trapped electrons at higher energies gives insufficient growth of the waves below one half of the electron cyclotron frequency and a nonlinear generation mechanism might be necessary to explain their presence even in this simple case.

1.   Introduction

[2]   The equatorial region of the Earth's magnetosphere is a natural laboratory where we can observe strong interactions of different particle populations with electromagnetic and electrostatic waves. Several types of natural wave emissions are generated in this region, for example equatorial noise below the local lower hybrid frequency [e.g., *Horne*, 2007; *Meredith et al.*, 2008; *Shprits*, 2009, and references therein], electron cyclotron harmonic waves [e.g., *Meredith et al.*, 2009, and references therein], and whistler-mode chorus [e.g., *Burtis and Helliwell*, 1969; *Dunckel and Helliwell*, 1969; *Burton and Holzer*, 1974; *Tsurutani and Smith*, 1974; *Santolík*, 2008; *Meredith et al.*, 2009; *Omura et al.*, 2009; *Nunn et al.*, 2009].

[3]   The latter type of wave emissions, whistler-mode chorus, has been suggested to act as an accelerator of MeV electrons in the outer Van Allen radiation belt [e.g., *Horne and Thorne*, 1998; *Summers et al.*, 1998; *Horne et al.*, 2005; *Li et al.*, 2007; *Horne*, 2007; *Omura et al.*, 2007; *Albert et al.*, 2009; *Kasahara et al.*, 2009]. The mechanisms and effects of this process have been recently reviewed by *Shprits et al.* [2008] and *Vainio et al.* [2009]. Chorus is generated by instabilities of electron populations at energies from a few keV to a few tens of keV [e.g., *Tsurutani and Smith*, 1974; *Trakhtengerts et al.*, 2007; *Katoh and Omura*, 2007; *Omura et al.*, 2008, 2009; *Nunn et al.*, 2009]. Two

[1]Department of Space Physics, Institute of Atmospheric Physics, Prague, Czech Republic.
[2]Faculty of Mathematics and Physics, Charles University, Prague, Czech Republic.
[3]Department of Physics and Astronomy, University of Iowa, Iowa City, Iowa, USA.
[4]Mullard Space Science Laboratory, Holmbury St. Mary, UK.
[5]LPC2E, CNRS, Orléans, France.
[6]Station de Radioastronomie de Nancay, Observatoire de Paris, CNRS, Nancay, France.
[7]Laboratoire de Physique des Plasmas, CNRS, Palaiseau, France.
[8]Laboratoire Atmosphères, Milieux, Observations Spatiales, CNRS, Paris, France.
[9]Institute of Geophysics and Planetary Physics, University of California, Los Angeles, California, USA.
[10]Physical Sciences Division, British Antarctic Survey, Natural Environment Research Council, UK.

possibilities for unstable features of electron phase space distributions have been analyzed in the source region: a large temperature anisotropy [e.g., *Omura et al.*, 2009; *Nunn et al.*, 2009] or a step-like deformation of the electron velocity distribution in the direction parallel to the terrestrial magnetic field [*Trakhtengerts et al.*, 1996, 2004, 2007]. Based on early experimental results [*Burton and Holzer*, 1974], studies on generation of chorus often assume that the waves are generated with quasi-parallel wave vectors with respect to the terrestrial magnetic field. However, both theoretical [*Bell*, 1984, 1986; *Albert*, 2008; *Shklyar and Matsumoto*, 2009] and experimental [*Parrot and Lefeuvre*, 1986; *Tsurutani et al.*, 2009; *Verkhoglyadova et al.*, 2009; *Chum et al.*, 2009; *Santolík et al.*, 2009] studies suggest that oblique propagation might be important, at least in some cases.

[4] Whistler-mode chorus is usually composed of discrete wave packets but it is often accompanied by a random shapeless hiss at lower frequencies or in the chorus frequency band [*Dunckel and Helliwell*, 1969; *Burtis and Helliwell*, 1976; *Cornilleau-Wehrlin et al.*, 1978; *Koons*, 1981; *Hattori et al.*, 1991]. Alternating time intervals of hiss and discrete chorus elements have also been observed [*Tsurutani et al.*, 2009; *Santolík et al.*, 2009]. While the analysis of the source mechanism of the discrete wave packets requires a nonlinear theory [e.g., *Trakhtengerts and Rycroft*, 2008; *Omura et al.*, 2009; *Nunn et al.*, 2009], it can be possible to explain the associated hiss emissions using a linear or quasilinear stability and diffusion analysis [*Cornilleau-Wehrlin et al.*, 1985; *Solomon et al.*, 1988]. The aim of the present paper is to investigate linear wave-particle interactions in the equatorial source region of whistler-mode emissions. Our analysis is based on observations of the Cluster spacecraft mission. We select a case of wave emissions which predominantly occur in the form of weak random hiss. The source is determined from the divergence of the measured Poynting flux.

[5] Section 2 presents our measurements of electromagnetic waves, and section 3 shows results of initial analysis of wave properties with the in-situ measurements of plasma parameters. Based on the measured electron phase space densities, presented in section 4, we show that obliquely propagating waves at frequencies above one half of the electron cyclotron frequency ($\frac{1}{2} f_{ce}$) are consistent with a linear instability of highly anisotropic electrons at energies of a few hundreds eV to a few keV. Our model of electron phase space densities, however, results in insufficient linear convective growth of waves below $\frac{1}{2} f_{ce}$. A companion paper by *Schriver et al.* [2010] shows that for the parameters of this event, non-linear mechanisms can transfer power from the wave above $\frac{1}{2} f_{ce}$ to lower frequencies by a wave-wave interaction.

2. Observations of Whistler-Mode Emissions in the Equatorial Source Region

[6] Figure 1 shows an overview of measurements of whistler-mode waves during a passage of the Cluster spacecraft through the equatorial region on 24 July 2003. The data are shown for Cluster 4 but all the four Cluster spacecraft provide us with a similar global picture since they are located within a few thousands of km apart. In this case the equatorial region is investigated just outside of the

plasmapause in the afternoon-sector, during a moderate geomagnetic activity with the maximum Kp index of 3+ and with the minimum DST index of −25 nT during the preceding 24 hours. The substorm activity is, however, non-negligible, with the AE index of 210 nT, reaching ≈700 nT four hours before the measurement, similar to events of High-Intensity Long-Duration Continuous AE Activity (HILDCAA) [*Tsurutani et al.*, 2009].

[7] A frequency-time power spectrogram of the electric field fluctuations (Figure 1a) has been obtained from the waveform measurements of the wide-band data (WBD) instrument [*Gurnett et al.*, 2001]. It demonstrates the presence of intense whistler-mode wave emissions in the beginning of the analyzed time interval. Most of the observed wave power is found between 1 and 4 kHz, which means below the locally measured $\frac{1}{2} f_{ce}$ shown as a white line in Figure 1a. After 1:00 UT the wave intensity in this band decreases and other weaker wave emissions occur in the band above $\frac{1}{2} f_{ce}$. After 1:30 UT the upper band decreases its frequency and after 1:50 UT it joins the lower band below $\frac{1}{2} f_{ce}$. At lower frequencies of a few hundreds of hertz a steady wave emission is present during the entire analyzed interval. All these waves are right hand polarized (not shown) and thus consistent with propagation in the electromagnetic whistler mode.

[8] Figure 1b represents the sum of three power spectra based on measurements of three-axial search-coil antennas processed by the onboard spectrum analyzer of the spatio-temporal analysis of field fluctuations (STAFF) instrument [*Cornilleau-Wehrlin et al.*, 2003]. The vertical white stripe occurring after 01:15 UT corresponds to a data gap. The resulting frequency-time power spectrogram of the magnetic field fluctuations demonstrates the electromagnetic nature of the observed waves in the lower frequency band below $\frac{1}{2} f_{ce}$. The parallel component of the Poynting vector normalized by its standard deviation (Figure 1c) has been calculated from the STAFF data based on measurement of both the electric and magnetic antennas. It shows that, before 1:24 UT, waves between 1 and 4 kHz (upper frequency limit of the instrument) propagate with a significant component antiparallel to the magnetic field direction, and that, after 1:24 UT these waves have a significant parallel component of the Poynting vector. As the spacecraft moves from the Southern hemisphere through the magnetic equator to the North, the observed properties correspond to a positive divergence of the Poynting flux around 1:24 UT where we expect the central position of the source region of the observed waves.

[9] This result can be compared to the position where the magnetic equator is detected using four-point vector measurements of the static magnetic field ($\mathbf{B}_0$) by the fluxgate magnetometers (FGM) onboard the four Cluster spacecraft [*Balogh et al.*, 2001]. This position is defined by the minimum of the magnetic field strength along the field line. We use a method described in the appendix of *Santolík et al.* [2009] and we find the zero derivative of the magnetic field strength at 01:24:21 UT for Cluster 4 (see Figure 1f), which means at the same time when we detect the central position of the source region from the Poynting vector measurements. At that position Figure 1d shows a small angle θ_{BK} between the wave vector and $\mathbf{B}_0$. This angle is calculated by the singular value decomposition method
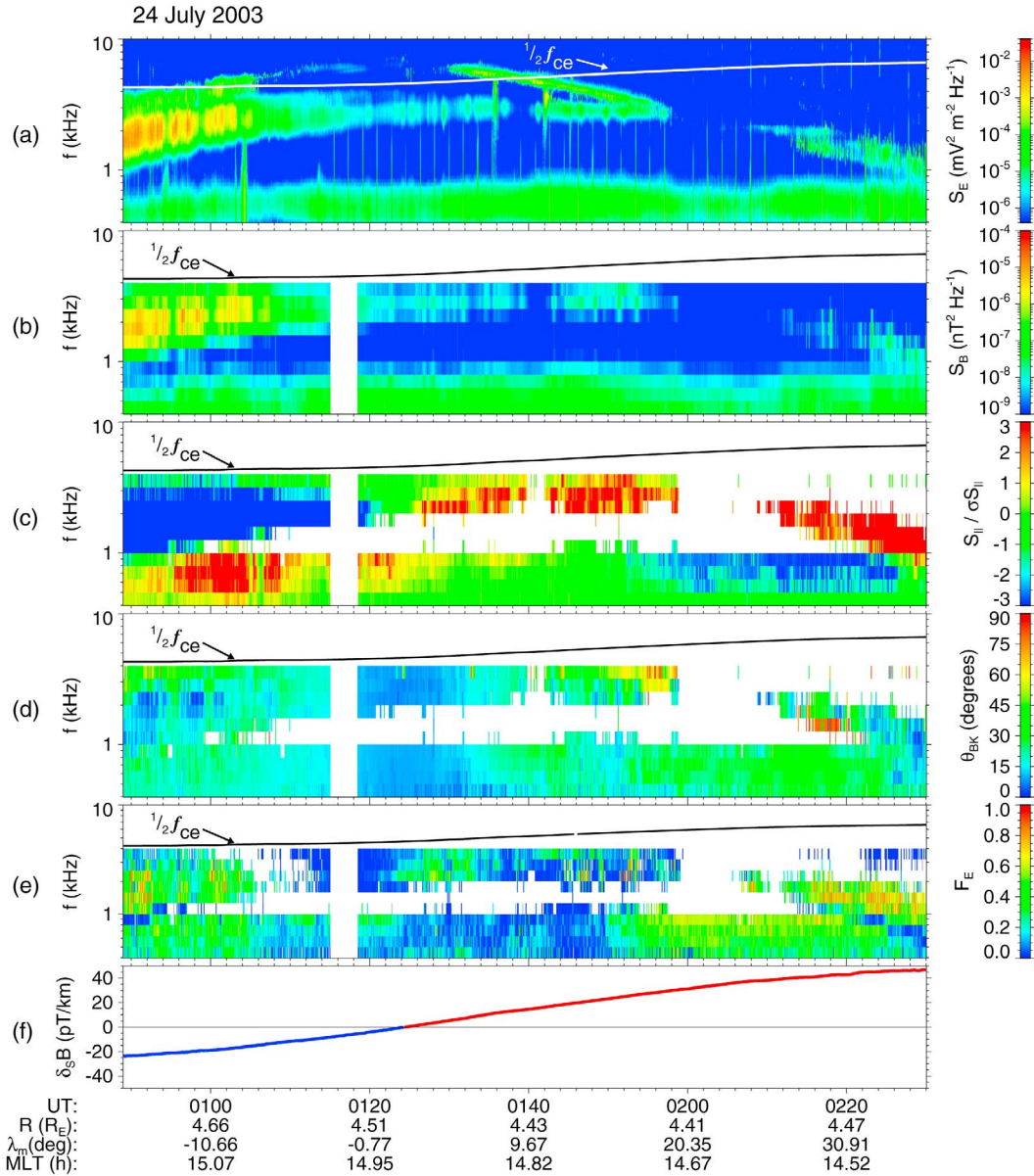
Figure 1. Measurements of Cluster 4 on 24 July 2003. (a) Power-spectral density of one component of electric field fluctuations in the plane perpendicular to the spacecraft spin axis; (b) sum of power-spectral densities of three orthogonal components of magnetic field fluctuations - the vertical white stripe occurring between 0115:00 and 0118:30 UT corresponds to a data gap; (c) parallel component of the Poynting vector normalized by its standard deviation; (d) angle between the wave vector and $\mathbf{B}_0$ supposing the plane wave model; (e) electromagnetic planarity; (f) spatial gradient of $|\mathbf{B}_0|$ projected on the local field line from four-point measurements; Solid lines plotted over Figures 1a–1e show one half of the electron cyclotron frequency from local measurements of the static magnetic field. Position of Cluster 4 is given on the bottom: R - radial distance in Earth's radii, λ_m - magnetic dipole latitude in degrees, MLT - magnetic local time in hours.

[Santolík et al., 2003] from the STAFF magnetic field measurements. If the underlying hypothesis of the presence of a single plane wave is valid, the results at the central position of the source region would correspond to quasi-parallel propagation with $\theta_{BK} < 15°$. Note that θ_{BK} increases significantly further out from the central position of the source region.

[10] The electromagnetic planarity [Santolík et al., 2003] is also low ($F_E < 0.2$) in the source region (see Figure 1e). This parameter characterizes the degree of similarity of the wave polarization with the ideal polarization of a single plane wave. Our results therefore indicate simultaneous presence of plane waves propagating in different directions. F_E increases above 0.8 further out from the central position of the source region, where the waves only propagate in the
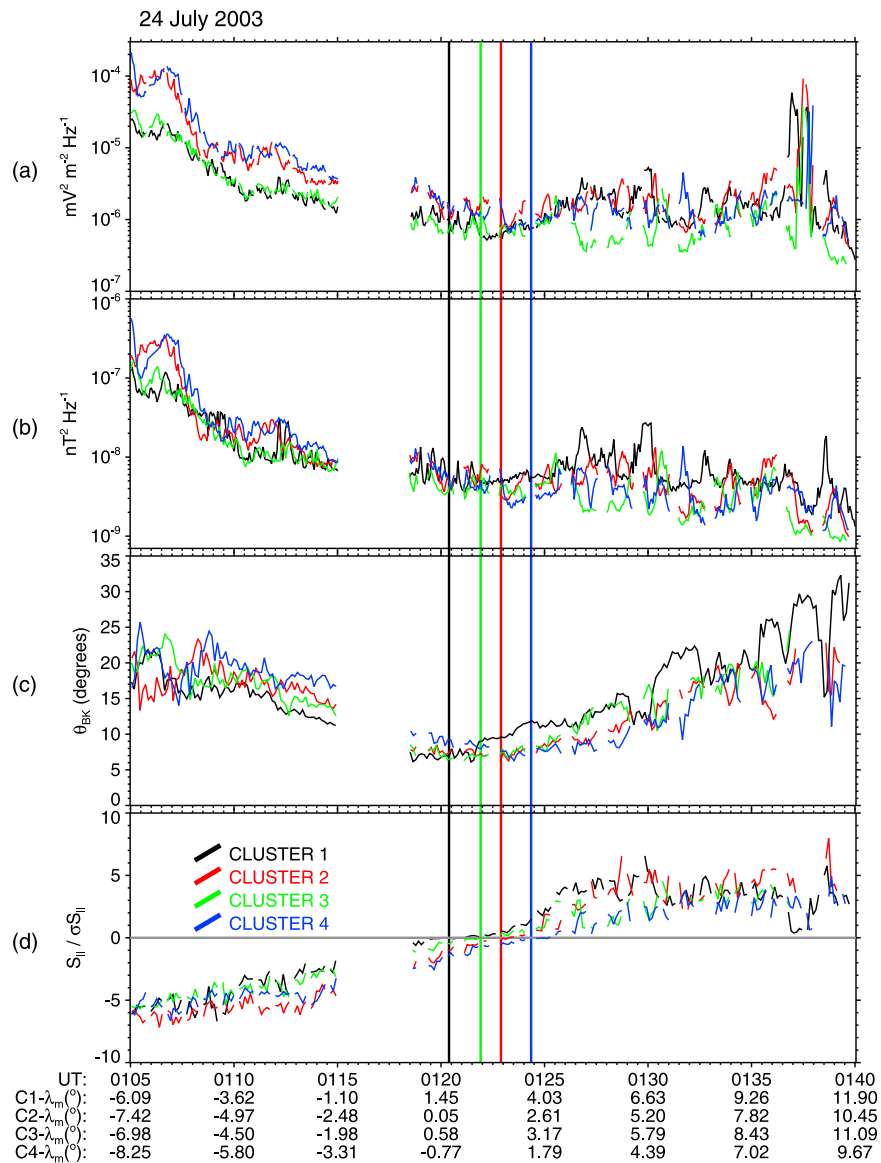
Figure 2. Parameters of waves analyzed in their source region by the STAFF instrument on 24 July 2003. Average values for the frequency range 1.6–4 kHz. (a) Sum of power-spectral densities of the two measured components of the electric field fluctuations in the spacecraft spin plane; (b) sum of power-spectral densities of three orthogonal components of the magnetic field fluctuations; (c) angle between the wave vector and $\mathbf{B}_0$; (d) parallel component of the Poynting vector normalized by its standard deviation; The data from the four Cluster spacecraft are color-coded according to the legend on the left-hand side of Figure 2d. The vertical solid lines drawn over Figures 2a–2d show the times when each spacecraft passes through the measured magnetic field minimum along the field line. Dipole magnetic latitude (λ_m) in degrees is given on the bottom for the four Cluster spacecraft.

direction outward from the source. Note that waves at frequencies below 1 kHz show an inverse propagation pattern in Figure 1c, i.e., they propagate toward the magnetic equator. This most probably corresponds to magnetospherically reflected chorus described by *Parrot et al.* [2003, 2004].

[11] Figure 2 shows average values of wave characteristics in the frequency range 1.6–4 kHz for all four Cluster spacecraft. The results are plotted in a narrower time interval centered around the passages of the four spacecraft through the minima of the magnetic field modulus along the

corresponding field lines. The minima are shown by vertical lines and occur at a dipole magnetic latitude of 1.6°. They are again calculated separately for each spacecraft from the four-point FGM measurements using the method from the appendix of *Santolík et al.* [2009]. Cluster 1, 2, 3 and 4 respectively pass through these minima at 01:20:23, 01:22:54, 01:21:55, and 01:24:21 UT. The largest time separation occurs between Cluster 1 and Cluster 4, and corresponds to their separation of approximately 1000 km along the magnetic field line. The separation of the space-
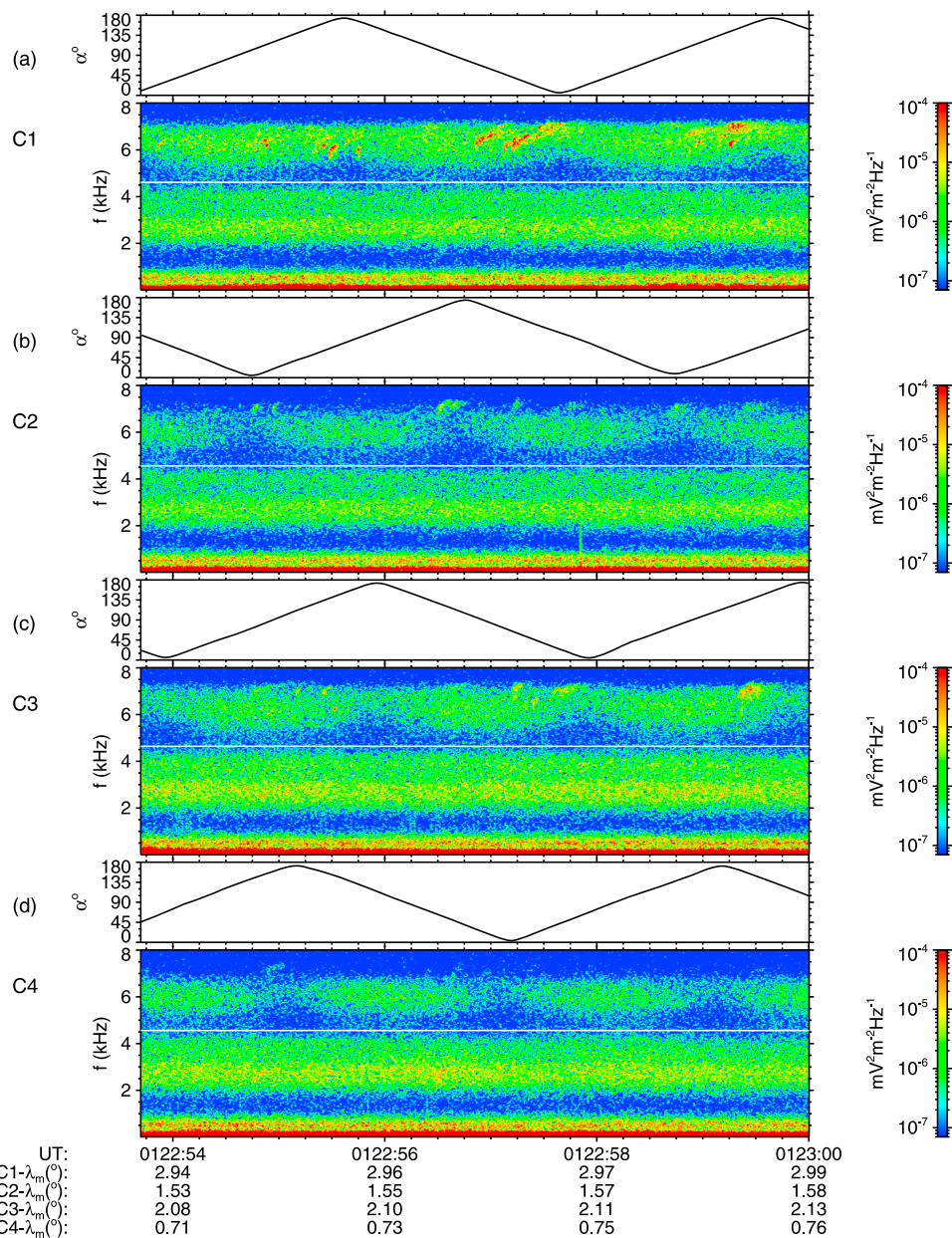
Figure 3. (a–d) High-resolution spectrograms of the power-spectral density calculated from the electric field waveforms recorded by the WBD instruments on board the Cluster 1–4 spacecraft on 24 July 2003. Angle α between the electric antenna and the x_{GSE} direction is given on the top of each spectrogram. The selected 6-s time interval corresponds to the passage of Cluster 2 through the central position of the source region. The solid lines plotted over the spectrograms show one half of the electron cyclotron frequency from local measurements. Magnetic dipole latitudes (λ_m) of the four spacecraft are given on the bottom.

craft across the magnetic field lines is smaller, between a few tens and a few hundreds km.

[12] In Figures 2a and 2b we can notice the final part of the decrease of the wave power before the passage of the individual spacecraft through the central position of the source. At that position we observe weak waves with electric-field power-spectral densities between 6×10^{-7} and 2×10^{-6} mV^2 m^{-2} Hz^{-1} (Figure 2a), while the magnetic-field power-spectral densities are roughly estimated as $2–8 \times 10^{-9}$ nT^2 Hz^{-1} (Figure 2b). These values give the dimen-

sionless ratio of the magnetic to electric power, $c^2 B^2 / E_s^2 \approx 90–1200$, where c is the speed of light, and E_s is the electric field component perpendicular to the spacecraft spin axis.

[13] Figure 2c clearly shows that θ_{BK} obtained from measurements of each of the spacecraft reach their minimum values of 7° when the respective spacecraft pass through central position of the source. Finally, Figure 2d demonstrates for each spacecraft separately that this position indeed corresponds to the point where the parallel component of the Poynting vector passes through zero. This pat-
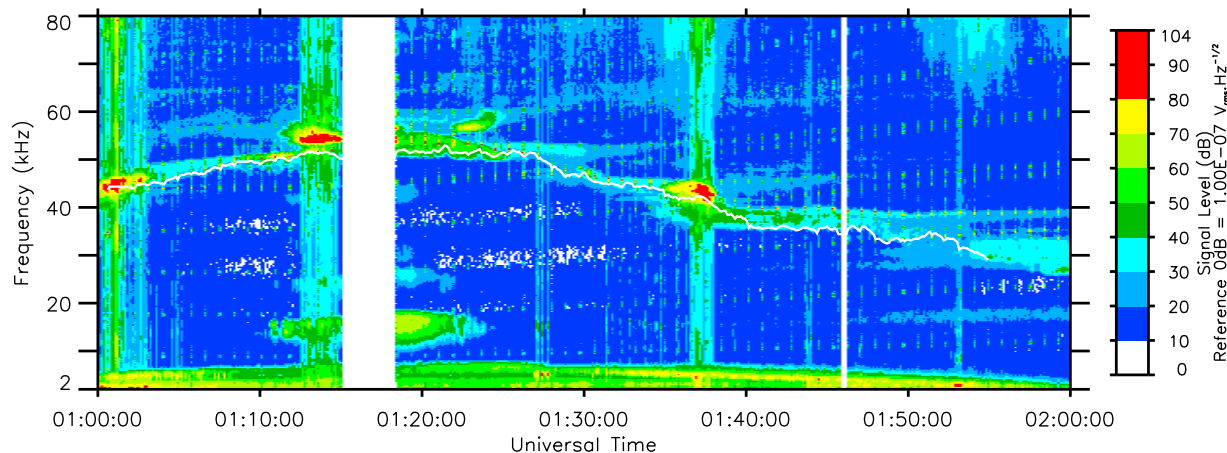
Figure 4. Frequency-time spectrogram of the electric field in the frequency range from 2 to 80 kHz obtained on 24 July 2003 by the WHISPER instrument onboard Cluster 1. White line shows an estimate of the local plasma frequency.

tern, both for θ_{BK} and for the Poynting vector, is remarkably repetitive for the successive passages of the four spacecraft through the minima of the magnetic field modulus.

[14] To investigate details of the frequency-time evolution of the wave power in the source region we process the high-resolution waveforms of the electric field acquired by the WBD instrument. The results are shown in Figure 3 over a short time interval of 6 s when Cluster 2 passes through the central position of the source region. Similar results have been obtained for other time intervals inside the source region, for example when the other three Cluster spacecraft pass through the central position of the source region.

[15] At low frequencies below 1 kHz all the four spacecraft observe intense emissions of equatorial noise and reflected whistler-mode waves. At frequencies above 2 kHz weaker whistler-mode waves show up as shapeless hiss without any clear modulation or discrete structures. This type of wave is present in the frequency range from 0.2 to 0.5 f_{ce}, with a maximum wave power around 0.3 f_{ce}. At and slightly above 0.5 f_{ce} we observe a narrow band of decreased wave intensity that is often present in whistler-mode chorus emissions, and whose origin is a subject of active investigation [*Bell et al.*, 2009; *Omura et al.*, 2009].

[16] At higher frequencies, in a band between 0.5 to 0.8 f_{ce}, the emissions become more structured. Intense chorus wave packets with a growing frequency embedded in the background hiss occasionally occur in this band. The peak of average wave power is found around 0.65–0.7 f_{ce}. Note that the difference of frequencies observed on the different spacecraft is negligible, unlike the previously observed shifts of chorus wave packets in frequency and time which were found in other cases [e.g., *Gurnett et al.*, 2001; *Inan et al.*, 2004; *Platino et al.*, 2006; *Chum et al.*, 2007; *Breneman et al.*, 2009; *Chum et al.*, 2009; *Santolík et al.*, 2009].

[17] Intensity of background hiss above $\frac{1}{2}f_{ce}$ shows a regular modulation by the spacecraft spin. The minima systematically occur for the antenna orientation within a few tens of degrees from the sunward and/or anti-sunward direction. This modulation leads to the maximum power that is approximately 3–4 times larger than the minimum power,

if we integrate the spectrograms in Figure 3 over the upper frequency band from 4.5 to 8 kHz. Note that we are unable to examine the ratio of the electric to magnetic field wave amplitudes, since the magnetic field is not measured at frequencies above 4 kHz.

3. Analysis of Wave Polarization and Propagation Properties

[18] The modulation pattern of the electric-field power observed by a spinning antenna in a band between 0.5 to 0.8 f_{ce} can be explained by an elliptical polarization of the wave electric field, by an inclination of the normal to the polarization plane from the spacecraft spin axis, or by a combination of the two effects. For instance, if we first assume a nearly circular polarization, the normal to the electric field polarization plane would be inclined by approximately 55°–60° from the spacecraft spin axis to explain the observed modulation depth. As the measured $\mathbf{B}_0$ is only at ≈10°–15° from the spin axis, the normal to the electric field polarization plane would be also highly inclined from $\mathbf{B}_0$. However, in this situation we cannot reasonably assume the circular polarization. This simple example demonstrates that, to be able to infer the propagation properties from the observed spin pattern, we need a theoretical estimate of the expected wave polarization as a function of the wave vector direction. As the first step we use the cold-plasma theory [*Stix*, 1992] with experimentally observed parameters of the plasma medium: the electron cyclotron frequency obtained from magnetic field measurements by the FGM instrument [*Balogh et al.*, 2001] and the plasma frequency estimated from passive and active measurements of the WHISPER sounder [*Décréau et al.*, 2001].

[19] Figure 4 shows a frequency-time spectrogram of the electric field obtained by WHISPER onboard Cluster 1. The frequency range from 2 to 80 kHz allows us to detect the plasma frequency (f_p), which is identified as a resonance in WHISPER sounder's signatures, and as the lower cut off of locally enhanced background noise in the frequency band f_p - f_{UH}, where f_{UH} is the upper hybrid frequency [*Canu et*
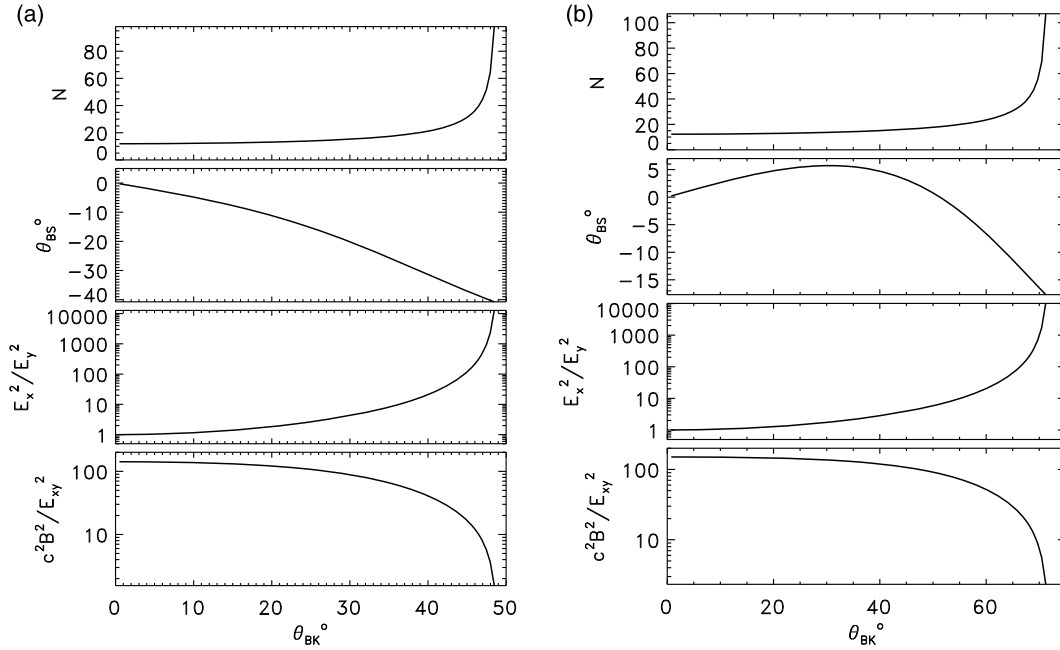
(a)

(b)

Figure 5. Results of the theoretical analysis of a whistler-mode wave at a frequency of (a) 6 kHz, and (b) 2.85 kHz in a cold plasma as a function of the angle θ_{BK} between the wave vector and $\mathbf{B}_0$. (top panel) the refractive index; (second panel) angle θ_{BS} between the group velocity and $\mathbf{B}_0$ – negative values are used for the opposite azimuth compared to the wave vector; (third panel) ratio of two components of the electric field power in the plane perpendicular to $\mathbf{B}_0$; (fourth panel) ratio of the magnetic field power versus the electric field power perpendicular to $\mathbf{B}_0$.

al., 2001]. The f_p estimate is shown by the white line in Figure 4. For the time interval from Figure 3 this estimate gives a plasma frequency of 52 kHz, corresponding to the plasma number density of 34 cm^{-3}. For the same time interval the FGM instrument gives a magnetic field strength of 330 nT corresponding to the electron cyclotron frequency $f_{ce} = 9.2$ kHz.

[20] The results of our calculations for the upper band of whistler-mode emissions are shown in Figure 5a. We use the wave frequency of 6 kHz (0.65 f_{ce}) which is the observed peak of the average wave power in this band. The refractive index increases with the angle θ_{BK} from $N = 11.9$ for the parallel propagation and diverges when θ_{BK} is at the resonance angle $\theta_R = 48.9°$. The wave frequency above $\frac{1}{2} f_{ce}$ implies the monotonically increasing angular inclination θ_{BS} of the group velocity vector from $\mathbf{B}_0$.

[21] The observations of the spin modulation in this band can be compared to the theoretical estimate E_x^2/E_y^2, where E_x and E_y are two electric field components in the plane perpendicular to $\mathbf{B}_0$. The E_x component is in the direction of the projection of the wave vector onto this plane, while E_y is perpendicular to both the wave vector and $\mathbf{B}_0$. The polarization is circular with $E_x^2/E_y^2 = 1$ only for the parallel propagation. For larger θ_{BK} the polarization changes to elliptical and E_x^2 significantly increases compared to E_y^2. The observed depth of spin modulation, with 3–4 times higher maximum wave power compared to the minimum, is reached for θ_{BK} between 25° and 30°.

[22] The spin modulation would quickly become much deeper for higher θ_{BK} if the spin axis was exactly aligned along $\mathbf{B}_0$. This is not exactly fulfilled in our case and we therefore cannot exclude that the real θ_{BK} is larger than 30°,

possibly even very close to the resonance angle. In that case, the electric field is linearly polarized along the wave vector, and the observed depth of spin modulation can still be explained by the existing deviation of the spin axis from $\mathbf{B}_0$ by 10°–15°. Our analysis nevertheless shows that θ_{BK} cannot be lower than ≈25°, which means ≈$\theta_R/2$.

[23] The dimensionless ratio of the wave magnetic field power to the power of the electric field component perpendicular to $\mathbf{B}_0$, c^2B^2/E_{xy}^2 is plotted on the lower-most panel of Figure 5a. It shows a strong relative decrease of the magnetic field fluctuations for higher θ_{BK}. We are unfortunately unable to compare this parameter with measurements since we do not measure the magnetic field spectra in the upper band of whistler-mode emissions, but we have these measurements at frequencies below 4 kHz.

[24] Figure 5b shows the same information as Figure 5a but for the frequency of 2.85 kHz (0.31 f_{ce}), i.e., at the peak of power in the lower band of the whistler-mode emissions. The refractive index increases with θ_{BK} from $N = 12.3$ for the parallel propagation. It diverges at the resonance angle $\theta_R = 71.7°$. The wave frequency is below $\frac{1}{2} f_{ce}$; the group velocity vector therefore has the same azimuth around $\mathbf{B}_0$ as the wave vector at low θ_{BK}. This is shown by small positive θ_{BS}. At the Gendrin angle $\theta_G = 51.2°$ the group velocity vector becomes field-aligned with $\theta_{BS} = 0$ and then it turns to negative values demonstrating the opposite azimuth compared to the wave vector.

[25] The ratios E_x^2/E_y^2 and c^2B^2/E_{xy}^2 in Figure 5b show similar behavior as we have discussed previously for higher frequencies (Figure 5a). However, we can now compare the calculated values of c^2B^2/E_{xy}^2 to the observations. From the measurements shown in Figures 2a and 2b we find (see
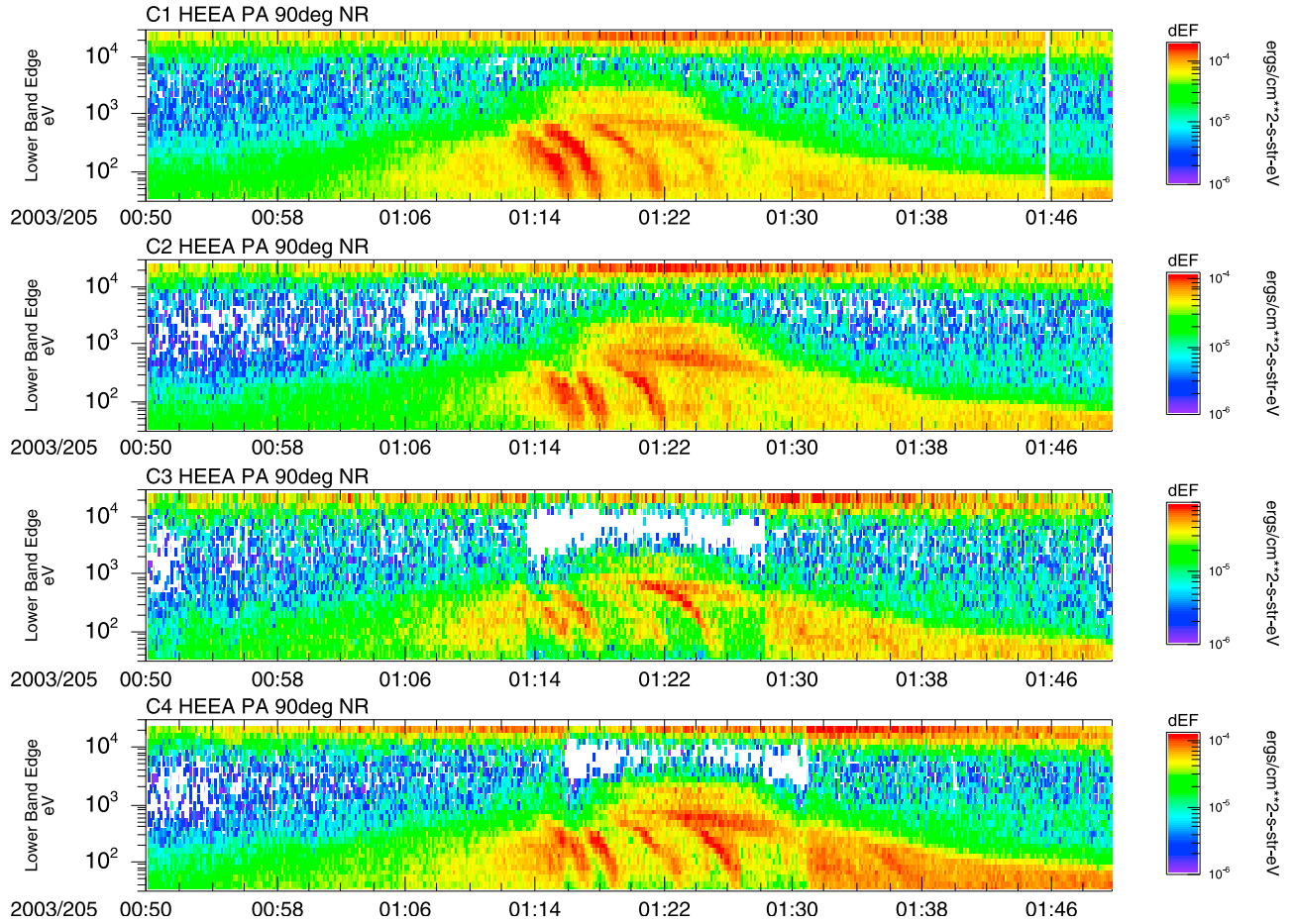
Figure 6. Dynamic energy spectrograms of differential energy flux of electrons measured perpendicular to the magnetic field line by the PEACE instruments onboard the four Cluster spacecraft (CL-1, CL-2, CL-3, and CL-4) on 24 July 2003.

section 2) a large range of $c^2 B^2/E_s^2$ between ≈ 90 to 1200. This value cannot be significantly influenced by the slight misalignment of the spin axis with respect to $\mathbf{B}_0$. Results in Figure 5b show that the wave vector in this frequency band can be parallel to $\mathbf{B}_0$, where we obtain $c^2 B^2/E_{xy}^2 = 150$ but that the observations can be also consistent with higher θ_{BK}. However, θ_{BK} cannot exceed $\approx 50°$, where $c^2 B^2/E_{xy}^2$ decreases below 90. For higher θ_{BK} we obtain too low relative power of the wave magnetic field which is not consistent with the observations.

4. Free Energy in the Electron Populations

[26] The obtained information on wave-normal directions of the observed waves as well as their spectra can be compared with theoretical properties of linear instabilities of the electron distribution functions in the source region. Figure 6 shows their differential energy flux at pitch angles close to perpendicular to $\mathbf{B}_0$ as a function of UT and energy. The data were measured by the Plasma Electron And Current Experiment (PEACE) [*Johnstone et al.*, 1997] onboard the four Cluster spacecraft.

[27] In the equatorial region, between 0050 and 0150 UT, an energetic electron population is detected above 10 keV. This is near the upper edge of the energy range of the

instrument at 26.7 keV, and therefore we observe only the lowest-energy part of this electron population which is probably trapped in the terrestrial magnetic field. Between 0115 and 0130 UT we can also notice intense energy-dispersed structures at energies from a few tens of eV up to a few keV. These structures occur at pitch angles close to perpendicular to the local field line. They are observed by the four spacecraft, though their shape is slightly different on each of the spacecraft. We have no explanation for the origin of the corresponding electron population at this moment since it is not probable that the electrons at these energies would drift all the way from night-side injections. The observed energy dispersion can be explained by a combination of the gradient-B drift with a partial corotation supposing a dayside source. No clear correspondence is found with measurements of electrons on the dayside at geosynchronous orbit (M. Thomsen, personal communication, 2009) by the Los Alamos National Laboratory MPA instruments [*Bame et al.*, 1993].

[28] Both the trapped energetic electrons and the injected electron population are co-localized with the source region of the whistler-mode emissions. To investigate the possibilities of the free energy for the wave generation we have analyzed complete electron pitch-angle distributions. We have used the data which are measured by the HEEA sensor
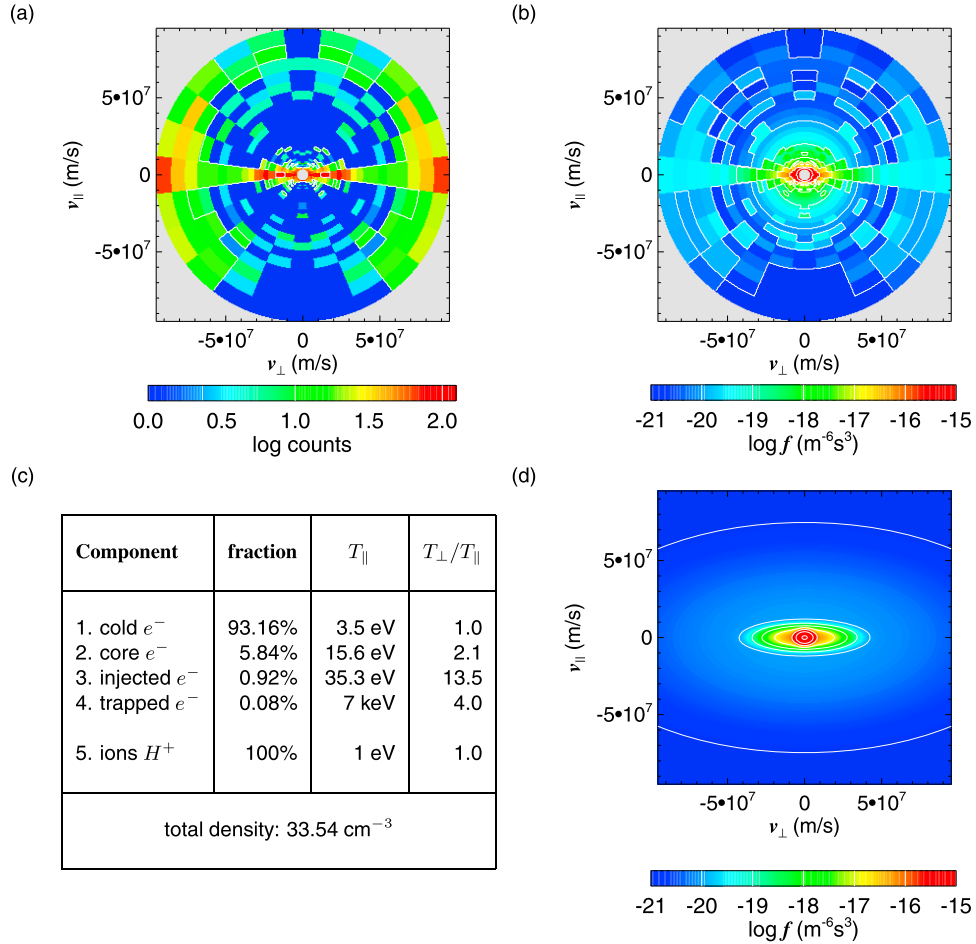
(a)

(b)

(c)

Component	fraction	$T_\parallel$	$T_\perp/T_\parallel$
1. cold e^-	93.16%	3.5 eV	1.0
2. core e^-	5.84%	15.6 eV	2.1
3. injected e^-	0.92%	35.3 eV	13.5
4. trapped e^-	0.08%	7 keV	4.0
5. ions H^+	100%	1 eV	1.0
total density: 33.54 cm^{-3}			

(d)

Figure 7. Electron distribution in velocities parallel ($v_\parallel$) and perpendicular ($v_\perp$) to the magnetic field line measured by the PEACE instrument onboard the Cluster 2 spacecraft on 24 July 2003 during four seconds (one spin period) centered at 0122:54. (a) total accumulated counts, (b) phase space density, (c) parameters of the fit, and (d) fit of the phase space density.

of the PEACE instrument once per spacecraft spin period of 4 s. This analysis has been done in the vicinity of the central position of the source region from 0110 to 0135 UT using the data from the four Cluster spacecraft. Figure 7 shows the results from Cluster 2 in a 4-s time interval around 0122:54 UT, which means at the central position of the source. The wave spectra for this time are presented in Figure 3b and have been discussed in section 2. The other electron pitch-angle distributions obtained within the source region are similar to those shown in Figure 7.

[29] Figure 7a represents counts accumulated by the instrument during 4 s in 13 pitch angle intervals and 30 logarithmic energy steps. The HEEA sensor collects measurements from a 180° field of view, divided into 12 zones of 15° each, every 0.125 s. Twice per spin the magnetic field lies in the plane of this field of view. The 13 pitch angle zones represent the minimum subset of the 24 zones which is needed to fully cover the pitch angle range, but some of the zones are collected half a spin before the others. The counts in Figure 7a are plotted as a function of the velocities parallel and perpendicular to $\mathbf{B}_0$ ($v_\parallel$ and $v_\perp$, respectively). We assume a gyrotropic distribution and the plot therefore has a mirror symmetry with respect to the line $v_\perp = 0$. We have

removed a background count level due to penetrating radiation which we were able to quantify using data from the LEEA and HEEA sensors together, taking advantage of their different sensitivity to plasma but near-identical response to penetrating energetic particles.

[30] Figure 7a indicates the presence of a low-energy core electron population and two highly anisotropic electron populations: the trapped energetic electrons detected in the highest two energy bins from 16.8 to 26.7 keV (velocities between 7.7×10^7 and 9.7×10^7 ms^{-1}), and the electrons linked to the dispersed structures at energies below 3 keV (at velocities below 3.2×10^7 ms^{-1}). These two populations have much higher $v_\perp$ compared to their $v_\parallel$ and the ratio of perpendicular to parallel temperatures $T_\perp/T_\parallel$ should thus be significantly larger than 1. The maximum counts in individual data accumulations reach nearly 130, and therefore we have sufficient counting statistics for the estimation of the phase space density. The result is shown in Figure 7b using the same type of plot with the same pitch-angle-energy bins as in Figure 7a.

[31] We estimate parameters of a three-component model of the electron phase space density consisting of three superposed bi-Maxwellian functions for three different
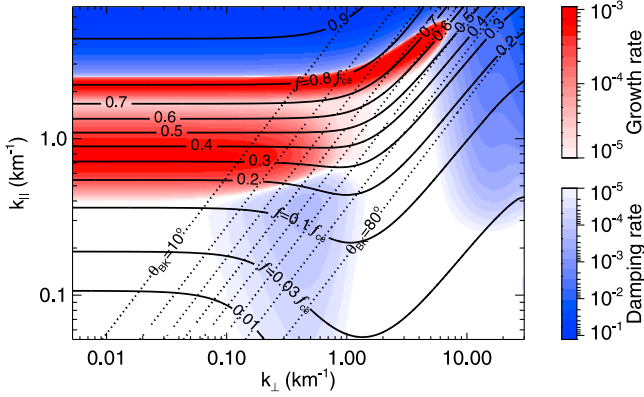
Figure 8. Results of the linear analysis of the wave dispersion using the "Waves in homogeneous, anisotropic multi-component plasmas" (WHAMP) program with the model of the electron distribution based on measurements by the PEACE instrument onboard the Cluster 2 spacecraft on 24 July 2003. Solid black lines show the ratio of wave frequency to f_{ce} in the plane defined by the wave vector components perpendicular and parallel to $\mathbf{B}_0$. Dotted lines correspond, from the left, to constant angles $\theta_{BK} = 10°$, 20°, 30°, …, 80°. The wave growth rate $\Im f/f_{ce}$ between 10^{-5} and 0.001, and the wave damping rate $-\Im f/f_{ce}$ between 10^{-5} and 0.13 are indicated on logarithmic color scales.

electron populations. We use a non-linear least squares estimate by a gradient-expansion algorithm based on the measured data in Figure 7b. The method gives us optimized values of number densities, $T_{\|}$, and $T_{\perp}/T_{\|}$ for the three populations. The resulting model is shown in Figure 7d and its parameters are given as components 2–4 ("core", "injected", "trapped") in the table 7c. Since we observe only the lowest energies of the "trapped" population of energetic electrons, the full optimization of both $T_{\|}$ and $T_{\perp}/T_{\|}$ is difficult to obtain for this component. We therefore manually adjust $T_{\perp}/T_{\|}$ to a fixed value of 4 which well corresponds to the observed shape of the electron distribution and to other optimization runs with a fixed $T_{\|}$. The relative errors of the model parameters based on the counting statistics are 3–7% for the number densities and 2–8% for $T_{\|}$. The lowest errors are always obtained for the "core" population and the largest ones for the "trapped" energetic electrons. The statistical errors of the optimization procedure for $T_{\perp}/T_{\|}$ are 2% and 4% for the "core" and "injected" populations, respectively.

[32] The sum of resulting number densities in these three components corresponds to 6.84% of the total plasma density which was found by the WHISPER sounder and which is shown in Figure 4. The reason why this is such a small percentage of the overall density is because our analysis is based only on the HEEA sensor which does not measure the lowest energies below 32 eV. We therefore add 93.16% of "cold" Maxwellian electrons. Their temperature is estimated using the data of the LEEA sensor to ≈3.5 eV. We have also added 1-eV protons as a neutralizing background to our plasma model.

[33] This model, together with the measured electron cyclotron frequency $f_{ce} = 9.2$ kHz (see section 3) is used for

theoretical calculations of the wave dispersion and stability using the "Waves in homogeneous, anisotropic multicomponent plasmas" (WHAMP) program [*Rönnmark*, 1982, 1983]. The procedure consists in resolution of the hot-plasma dispersion relation, providing us with a complex wave frequency as a function of a real wave vector. The real part of the frequency $R_E f$ then describes wave dispersion properties and the imaginary part of the frequency $\Im f$ brings information on the wave stability. Note that a finer analysis of $\Im f$ can be done using direct anisotropy calculations from the measured phase space densities [*Cornilleau-Wehrlin et al.*, 1985; *Solomon et al.*, 1988] or by adding finer details to the model.

[34] Figure 8 shows the results of the WHAMP program plotted in the plane defined by the wave vector components perpendicular and parallel to $\mathbf{B}_0$, $k_{\perp}$ and $k_{\|}$, respectively. Note that we define these components to have the wave number $k = 2\pi/\lambda = \sqrt{k_{\perp}^2 + k_{\|}^2}$, where λ is the wavelength, and to have $\theta_{BK} = \arctan(k_{\perp}/k_{\|})$.

[35] The ratio $R_E f/f_{ce}$ between 0.01 and 0.9 is plotted by the solid black lines. For frequencies above the lower hybrid frequency $f_{lh} = 0.023 f_{ce}$ the dispersion properties are characterized by the resonance cone shown by the oblique lines of constant frequency at $k_{\perp} > 1$ km^{-1}. The lines of constant θ_{BK} between 10° and 80° with a step of 10° are represented by the system of oblique dotted lines. The shading shows the ratio $\Im f/f_{ce}$ that reflects the effects of hot plasma on the linear growth or attenuation of wave amplitudes.

[36] For quasiparallel propagation at lowest $k_{\perp} < 0.01$ km^{-1} we first find stable waves at frequencies below $0.1 f_{ce}$, then two regions of wave growth. The first region has a broader peak in frequency with a maximum growth $\Im f/f_{ce} = 6.4 \times 10^{-4}$ at $k_{\|} = 0.77$ km^{-1}, and at a frequency of $0.33 f_{ce}$. This peak is related to the trapped population of energetic electrons. The calculated group speed for the maximum growth is 0.11 c, where c is the speed of light. This gives the length over which the wave amplitude convectively increases e times ("e-folding" length), $L_e \approx 5600$ km.

[37] The second, narrower amplification region for quasiparallel propagation has a very similar maximum growth $\Im f/f_{ce} = 6.6 \times 10^{-4}$ at $k_{\|} = 2.2$ km^{-1}, and at a frequency of $0.80 f_{ce}$. This peak is related to the injected population at lower energies. The group speed at this frequency is 0.026 c, which means that it is lower than in the previous case, and this corresponds to a lower e-folding length, $L_e \approx 1300$ km. At frequencies higher than $0.83 f_{ce}$ the waves start to be strongly attenuated.

[38] Both peaks are very broad in $k_{\perp}$. The wave growth at lower frequencies, however, disappears for $\theta_{BK} > 30$–40°. The peak at higher frequencies further intensifies for higher $k_{\perp}$, closer to the resonance cone. The maximum growth $\Im f/f_{ce} = 1.1 \times 10^{-3}$ is reached at $k_{\|} = 3.83$ km^{-1} and $k_{\perp} = 3.56$ km^{-1}. This point corresponds to $\theta_{BK} = 43°$ and to a frequency of $0.70 f_{ce}$. This is close to the resonance angle $\theta_R = 45.1°$ but still the propagation is not quasi resonant and the group speed is 0.023 c, which is only slightly lower than for the parallel propagating waves. With the increased growth rate, however, it gives a low convective e-folding length, $L_e \approx 680$ km. At the $k_{\|} = 3.83$ km^{-1} where we find the maximum growth this peak extends in frequency from

$0.5f_{ce}$ to $0.8f_{ce}$. It is again related to the injected population at energies below a few keV.

5. Discussion and Conclusions

[39] Results shown in section 4 indicate that both the highly anisotropic injected electrons at energies below a few keV and the trapped energetic electrons above 10 keV can amplify whistler mode waves. The energetic electrons would give rise to lower-band waves at frequencies below $\frac{1}{2} f_{ce}$, while the injected electrons would be responsible for the upper-band emissions above $\frac{1}{2} f_{ce}$, as we show them in Figure 3. We need, however, to estimate if the obtained linear wave growth is high enough to explain the presence of waves. For this rough estimate, we will, based on Figures 1 and 3, assume a reasonable lower limit for the necessary amplification: 4 orders of magnitude for the increase of power, which means a factor of 100 for the amplitude growth. We therefore need at least 4.6 e-folding lengths to allow the linear convective amplification to increase the amplitudes by this factor.

[40] For the upper band emissions grown at $\theta_{BK} = 43°$ and at a frequency of $0.70f_{ce}$ it gives us a convective amplification length $L_{100} \approx 3127$ km ≈ 0.5 R_E. This value reasonably compares to the observed size of the source region parallel to the field lines which is at least 15° in latitude (Figures 1 and 2), which means its linear dimension is over 1 R_E at a radial distance of 4.5 R_E. L_{100} is also below theoretical estimates of the parallel source size [*Helliwell*, 1967; *Cornilleau-Wehrlin and Gendrin*, 1979]. As we show in Figure 5a, the group speed of the waves at $\theta_{BK} = 43°$ is at large angles $\theta_{BS} \approx 40°$ from the magnetic field line, and we need also a similar size of the global source perpendicular to the magnetic field lines. We observe the same source populations on all the Cluster spacecraft, but their separation is only a few hundreds km perpendicular to the field line. These direct multipoint measurements therefore cannot prove that the source populations occur within at least a few thousands of km transversally to $\mathbf{B}_0$. However, such large transverse dimension of global equatorial sources have been found in the ray tracing study of whistler mode chorus by *Hayosh et al.* [2010] so we can reasonably expect that the upper-band emissions between 0.5 and $0.8f_{ce}$ are locally generated by the observed injected electron population. Note that waves with a high θ_{BK} are fully consistent with the observed spin modulation above $\frac{1}{2} f_{ce}$ (Figure 3). The oblique propagation has also been confirmed by the Darwin simulation code, as it is described in the companion paper by *Schriver et al.* [2010]. Note that in this case, the first-order cyclotron resonance and Landau resonance (also known as Čerenkov or zero-order cyclotron resonance) often play the most important role [*Boskova et al.*, 1990].

[41] For the lower-band emissions below $\frac{1}{2} f_{ce}$ we find the maximum growth rate at $\theta_{BK} \approx 0$ and at a frequency of $0.33f_{ce}$. The increase of the wave power by 4 orders of magnitude requires a convective amplification length $L_{100} \approx$ 25760 km ≈ 4 R_E. This is larger than the expected dimensions of the equatorial source region and our calculation therefore indicates that the lower-band emissions cannot grow fast enough from the unstable energetic population. The problem could be linked to uncertainties of parameters: the measurement gives us only the lowest energies from this

population for which $T_\perp/T_\parallel$ is estimated to 4. Our calculations show that we would need a much larger (approximately three times) $T_\perp/T_\parallel$ to decrease the convective amplification length below 1 R_E. The lower-band emissions therefore do not seem to be generated by a linear convective process from the modeled energetic population. This result assumes that the limited time resolution of 4 s and the limited ranges and resolutions of energies and pitch angles of our measurements do not prevent us from detecting other highly unstable features of the energetic electron population that would quickly disappear when the waves are generated; for example the step-like distribution functions [*Trakhtengerts et al.*, 1996; *Trakhtengerts et al.*, 2004, 2007] and/or large instantaneous anisotropies.

[42] *Schriver et al.* [2010] came to the conclusion that the lower frequency wave modes below $\frac{1}{2} f_{ce}$ are non-linearly excited from the emissions above $\frac{1}{2} f_{ce}$. The wave vector directions obtained from the Darwin simulation of this nonlinear process are at high θ_{BK} close to the resonance cone. This could be a good explanation of the observations but our results based on the plane wave approximation (Figures 1d and 2c) show a quasiparallel propagation with very low $\theta_{BK} < 10°$ in the center of the source region. These results could be, however, biased by the assumption of the presence of a single plane wave that is used for estimating θ_{BK}.

[43] We have done a preliminary verification of the validity of this assumption by estimating the distribution of the wave energy density with respect to the wave-vector directions, the wave distribution function (WDF) defined by *Storey and Lefeuvre* [1979]. A peaked WDF in the direction of $\mathbf{B}_0$ would mean that the assumption of a single plane wave is valid. However, our preliminary results rather show that the wave energy density can be distributed over a wide range of azimuthal directions around $\mathbf{B}_0$, forming thus a ring at $\theta_{BK} \approx 40–50°$. In this case, the analysis based on the assumption of the presence of a single plane wave could place the wave vector direction very close to the direction of $\mathbf{B}_0$, which means close to the center of the ring. This shape of the WDF would be consistent with the observed $c^2 B^2/E_s^2$ ratio (see section 3) which gives θ_{BK} lower than 50°. The ring-shaped WDF would also reconcile the results presented in Figures 1d and 2c with the results of the companion paper by *Schriver et al.* [2010]. However, the analysis of the WDF is out of scope of this paper and it will be a subject of future work.

[44] The summary of our case study of wave-particle interactions in the equatorial source region of whistler-mode emissions in the evening-side inner magnetosphere ($L \approx 4.5$ and MLT ≈ 15 h) reads as follows:

[45] 1. The observed whistler-mode emissions have most of the time the appearance of shapeless hiss in both frequency bands below and above $\frac{1}{2} f_{ce}$, with only occasional discrete structures observed above $\frac{1}{2} f_{ce}$ and resembling chorus wave packets. However, propagation properties of the waves below $\frac{1}{2} f_{ce}$ are very similar to previously analyzed cases of whistler-mode chorus: we observe the divergence of the Poynting flux at the plane where the modulus of the magnetic field is minimum along the field line; we observe low values of the electromagnetic planarity in the source region; we observe low values of the plane-wave estimate of the wave-vector angle θ_{BK}, with a minimum in the center of

the source region. This similarity suggests that the generation mechanism of the observed shapeless whistler-mode emissions and discrete chorus can have common features.

[46] 2. The measured electron phase space densities show an injected population at energies of a few hundreds eV to a few keV. We model this population using a bi-Maxwellian distribution with very high temperature anisotropies. The linear theory based on this model shows that whistler-mode waves in the upper band above $\frac{1}{2} f_{ce}$ can convectively grow to the observed amplitudes at distances that are lower or comparable to the size of the source region. The most unstable waves are at large angles θ_{BK} close to the resonance cone. This is consistent with the observed spin modulation of the wave power.

[47] 3. The measurements of electron phase space densities also indicate the presence of trapped energetic electrons at energies above 10 keV. We use a rough bi-Maxwellian model of this population and we obtain a linear instability of quasi parallel propagating waves in the lower band below $\frac{1}{2} f_{ce}$. The model, however, results in an insufficient convective growth and a non-linear mechanism suggested by the companion paper [*Schriver et al.*, 2010] can explain the observations.

References

Albert, J. M. (2008), Efficient approximations of quasi-linear diffusion coefficients in the radiation belts, *J. Geophys. Res.*, *113*, A06208, doi:10.1029/2007JA012936.

Albert, J. M., N. P. Meredith, and R. B. Horne (2009), Three-dimensional diffusion simulation of outer radiation belt electrons during the 9 October 1990 magnetic storm, *J. Geophys. Res.*, *114*, A09214, doi:10.1029/2009JA014336.

Balogh, A., et al. (2001), The Cluster magnetic field investigation: overview of in-flight performance and initial results, *Ann. Geophys.*, *19*, 1207–1217.

Bame, S. J., et al. (1993), Magnetospheric plasma analyzer for spacecraft with constrained resources, *Rev. Sci. Instrum.*, *64*, 1026–1033.

Bell, T. F. (1984), The nonlinear gyroresonance interaction between energetic electrons and coherent VLF waves propagating at an arbitrary angle with respect to the Earth's magnetic field, *J. Geophys. Res.*, *89*, 905–918, doi:10.1029/JA089iA02p00905.

Bell, T. F. (1986), The wave magnetic field amplitude threshold for nonlinear trapping of energetic gyroresonant and Landau resonant electrons by nonducted VLF waves in the magnetosphere, *J. Geophys. Res.*, *91*, 4365–4379.

Bell, T. F., U. S. Inan, N. Haque, and J. S. Pickett (2009), Source regions of banded chorus, *Geophys. Res. Lett.*, *36*, L11101, doi:10.1029/2009GL037629.

Boskova, J., F. Jiricek, P. Triska, B. V. Lundin, and D. R. Shkliar (1990), A possible common nature of equatorial half-gyrofrequency VLF emissions and discrete plasmaspheric emissions, *Ann. Geophys.*, *8*, 755–763.

Breneman, A. W., C. A. Kletzing, J. Pickett, J. Chum, and O. Santolik (2009), Statistics of multispacecraft observations of chorus dispersion and source location, *J. Geophys. Res.*, *114*, A06202, doi:10.1029/2008JA013549.

Burtis, W. J., and R. A. Helliwell (1969), Banded chorus—A new type of VLF radiation observed in the magnetosphere by OGO 1 and OGO 3, *J. Geophys. Res.*, *74*, 3002–3010, doi:10.1029/JA074i011p03002.

Burtis, W. J., and R. A. Helliwell (1976), Magnetospheric chorus: Occurrence patterens and normalized frequency, *Planet. Space Sci.*, *24*, 1007–1024.

Burton, R. K., and R. E. Holzer (1974), The origin and propagation of chorus in the outer magnetosphere, *J. Geophys. Res.*, *79*, 1014–1023.

Canu, P., et al. (2001), Identification of natural plasma emissions observed close to the plasmapause by the Cluster-Whisper relaxation sounder, *Ann. Geophys.*, *19*, 1697–1709.

Chum, J., O. Santolik, A. W. Breneman, C. A. Kletzing, D. A. Gurnett, and J. S. Pickett (2007), Chorus source properties that produce time shifts and frequency range differences observed on different cluster spacecraft, *J. Geophys. Res.*, *112*, A06206, doi:10.1029/2006JA012061.

Chum, J., O. Santolik, D. A. Gurnett, and J. S. Pickett (2009), Oblique lower band chorus waves: Time shifts between discrete elements observed by the Cluster spacecraft, *J. Geophys. Res.*, *114*, A00F02, doi:10.1029/2009JA014366.

Cornilleau-Wehrlin, N., and R. Gendrin (1979), VLF transmitter-induced quiet bands: A quantitative interpretation, *J. Geophys. Res.*, *84*, 882–890, doi:10.1029/JA084iA03p00882.

Cornilleau-Wehrlin, N., R. Gendrin, F. Lefeuvre, M. Parrot, R. Grard, D. Jones, A. Bahnsen, E. Ungstrup, and W. Gibbons (1978), VLF electromagnetic waves observed onboard GEOS-1, *Space Sci. Rev.*, *22*, 371–382.

Cornilleau-Wehrlin, N., J. Solomon, A. Korth, and G. Kremser (1985), Experimental study of the relationship between energetic electrons and ELF waves observed on board GEOS: A support to quasi-linear theory, *J. Geophys. Res.*, *90*, 4141–4154, doi:10.1029/JA090iA05p04141.

Cornilleau-Wehrlin, N., et al. (2003), First results obtained by the Cluster STAFF experiment, *Ann. Geophys.*, *21*, 437–456.

Décréau, P. M. E., et al. (2001), Early results from the Whisper instrument on Cluster: An overview, *Ann. Geophys.*, *19*, 1241–1258.

Dunckel, N., and R. A. Helliwell (1969), Whistler-mode emissions on the OGO 1 Satellite, *J. Geophys. Res.*, *74*, 6371–6385, doi:10.1029/JA074i026p06371.

Gurnett, D. A., et al. (2001), First results from the Cluster wideband plasma wave investigation, *Ann. Geophys.*, *19*, 1259–1272.

Hattori, K., M. Hayakawa, D. Lagoutte, M. Parrot, and F. Lefeuvre (1991), Further evidence of triggering chorus emissions from wavelets in the hiss band, *Planet. Space Sci.*, *39*, 1465–1472, doi:10.1016/0032-0633(91) 90075-L.

Hayosh, M., O. Santolik, and M. Parrot (2010), Location and size of the global source region of whistler mode chorus, *J. Geophys. Res.*, *115*, A00F06, doi:10.1029/2009JA014950.

Helliwell, R. A. (1967), A theory of discrete emissions from the magnetosphere, *J. Geophys. Res.*, *72*, 4773–4790.

Horne, R. B. (2007), Acceleration of killer electrons, *Nat. Phys.*, *3*, 590–591.

Horne, R. B., and R. M. Thorne (1998), Potential waves for relativistic electron scattering and stochastic acceleration during magnetic storms, *Geophys. Res. Lett.*, *25*(15), 3011–3014, doi:10.1029/98GL01002.

Horne, R. B., et al. (2005), Wave acceleration of electrons in the Van Allen radiation belts, *Nature*, *437*, 227–230, doi:10.1038/nature03939.

Inan, U. S., M. Platino, T. F. Bell, D. A. Gurnett, and J. S. Pickett (2004), Cluster measurements of rapidly moving sources of ELF/VLF chorus, *J. Geophys. Res.*, *109*, A05214, doi:10.1029/2003JA010289.

Johnstone, A. D., et al. (1997), Peace: A plasma electron and current experiment, *Space Sci. Rev.*, *79*, 351–398, doi:10.1023/A:1004938001388.

Kasahara, Y., Y. Miyoshi, Y. Omura, O. P. Verkhoglyadova, I. Nagano, I. Kimura, and B. T. Tsurutani (2009), Simultaneous satellite observations of VLF chorus, hot and relativistic electrons in a magnetic storm "recovery" phase, *Geophys. Res. Lett.*, *36*, L01106, doi:10.1029/2008GL036454.

Katoh, Y., and Y. Omura (2007), Computer simulation of chorus wave generation in the Earth's inner magnetosphere, *Geophys. Res. Lett.*, *34*, L03102, doi:10.1029/2006GL028594.

Koons, H. C. (1981), The role of hiss in magnetospheric chorus emissions, *J. Geophys. Res.*, *86*, 6745–6754.

Li, W., Y. Y. Shprits, and R. M. Thorne (2007), Dynamic evolution of energetic outer zone electrons due to wave-particle interactions during storms, *J. Geophys. Res.*, *112*, A10220, doi:10.1029/2007JA012368.

Meredith, N. P., R. B. Horne, and R. R. Anderson (2008), Survey of magnetosonic waves and proton ring distributions in the Earth's inner magnetosphere, *J. Geophys. Res.*, *113*, A06213, doi:10.1029/2007JA012975.

Meredith, N. P., R. B. Horne, R. M. Thorne, and R. R. Anderson (2009), Survey of upper band chorus and ECH waves: Implications for the diffuse aurora, *J. Geophys. Res.*, *114*(A13), A07218, doi:10.1029/2009JA014230.

Nunn, D., O. Santolik, M. Rycroft, and V. Trakhtengerts (2009), On the numerical modelling of VLF chorus dynamical spectra, *Ann. Geophys.*, *27*, 2341–2359.

Omura, Y., N. Furuya, and D. Summers (2007), Relativistic turning acceleration of resonant electrons by coherent whistler mode waves in a dipole magnetic field, *J. Geophys. Res.*, *112*, A06236, doi:10.1029/2006JA012243.

Omura, Y., Y. Katoh, and D. Summers (2008), Theory and simulation of the generation of whistler-mode chorus, *J. Geophys. Res.*, *113*, A04223, doi:10.1029/2007JA012622.

Omura, Y., M. Hikishima, Y. Katoh, D. Summers, and S. Yagitani (2009), Nonlinear mechanisms of lower-band and upper-band VLF chorus emissions in the magnetosphere, *J. Geophys. Res.*, *114*, A07217, doi:10.1029/2009JA014206.

Parrot, M., and F. Lefeuvre (1986), Statistical study of the propagation characteristics of ELF hiss observed on GEOS-1, outside and inside the plasmasphere, *Ann. Geophys.*, *4*, 363–384.

Parrot, M., O. Santolík, N. Cornilleau-Wehrlin, M. Maksimovic, and C. Harvey (2003), Magnetospherically reflected chorus waves revealed by ray tracing with Cluster data, *Ann. Geophys.*, *21*, 1111–1120.

Parrot, M., O. Santolík, D. Gurnett, J. Pickett, and N. Cornilleau-Wehrlin (2004), Characteristics of magnetospherically reflected chorus waves observed by Cluster, *Ann. Geophys.*, *22*, 2597–2606.

Platino, M., U. S. Inan, T. F. Bell, J. S. Pickett, and P. Canu (2006), Rapidly moving sources of upper band ELF/VLF chorus near the magnetic equator, *J. Geophys. Res.*, *111*, A09218, doi:10.1029/2005JA011468.

Rönnmark, K. (1982), Waves in homogeneous, anisotropic multicomponent plasmas (WHAMP), technical report, Kiruna Geophys. Inst., Kiruna, Sweden.

Rönnmark, K. (1983), Computation of the dielectric tensor of a Maxwellian plasma, *Plasma Phys.*, *25*, 699–701, doi:10.1088/0032-1028/25/6/007.

Santolík, O. (2008), New results of investigations of whistler-mode chorus emissions, *Nonlin. Proc. Geophys.*, *15*, 621–630.

Santolík, O., M. Parrot, and F. Lefeuvre (2003), Singular value decomposition methods for wave propagation analysis, *Radio Sci.*, *38*(1), 1010, doi:10.1029/2000RS002523.

Santolík, O., D. A. Gurnett, J. S. Pickett, J. Chum, and N. Cornilleau-Wehrlin (2009), Oblique propagation of whistler mode waves in the chorus source region, *J. Geophys. Res.*, *114*, A00F03, doi:10.1029/2009JA014586.

Schriver, D., et al. (2010), The generation of whistler mode chorus emissions in the inner magnetosphere: An event study, *J. Geophys. Res.*, doi:10.1029/2009JA014932, in press.

Shklyar, D., and H. Matsumoto (2009), Oblique whistler-mode waves in the inhomogeneous magnetospheric plasma: Resonant interactions with energetic charged particles, *Surv. Geophys.*, *30*, 55–104, doi:10.1007/s10712-009-9061-7.

Shprits, Y. Y. (2009), Potential waves for pitch-angle scattering of nearequatorially mirroring energetic electrons due to the violation of the second adiabatic invariant, *Geophys. Res. Lett.*, *36*, L12106, doi:10.1029/2009GL038322.

Shprits, Y. Y., D. A. Subbotin, N. P. Meredith, and S. R. Elkington (2008), Review of modeling of losses and sources of relativistic electrons in the outer radiation belt II: Local acceleration and loss, *J. Atmos. Sol. Terr. Phys.*, *70*, 1694–1713, doi:10.1016/j.jastp.2008.06.014.

Solomon, J., N. Cornilleau-Wehrlin, A. Korth, and G. Kremser (1988), An experimental study of ELF/VLF hiss generation in the Earth's magnetosphere, *J. Geophys. Res.*, *93*, 1839–1847, doi:10.1029/JA093iA03p01839.

Stix, T. H. (1992), *Waves in Plasmas*, Am. Inst. of Phys., New York.

Storey, L. R. O., and F. Lefeuvre (1979), The analysis of 6-component measurement of a random electromagnetic wave field in a magnetoplasma, 1, The direct problem, *Geophys. J. R. Astron. Soc.*, *56*, 255–270.

Summers, D., R. M. Thorne, and F. Xiao (1998), Relativistic theory of waveparticle resonant diffusion with application to electron acceleration in the magnetosphere, *J. Geophys. Res.*, *103*(A9), 20,487–20,500.

Trakhtengerts, V. Y., and M. J. Rycroft (2008), *Whistler and Alfvén Mode Cyclotron Masers in Space*, Cambridge Univ. Press, Cambridge, U. K.

Trakhtengerts, V. Y., M. J. Rycroft, and A. G. Demekhov (1996), Interrelation of noise-like and discrete ELF/VLF emissions generated by cyclotron interactions, *J. Geophys. Res.*, *101*, 13,293–13,301, doi:10.1029/95JA03515.

Trakhtengerts, V. Y., A. G. Demekhov, E. E. Titova, B. V. Kozelov, O. Santolik, D. Gurnett, and M. Parrot (2004), Interpretation of Cluster data on chorus emissions using the backward wave oscillator model, *Phys. Plasmas*, *11*, 1345–1351.

Trakhtengerts, V. Y., et al. (2007), Formation of vlf chorus frequency spectrum: Cluster data and comparison with the backward wave oscillator model, *Geophys. Res. Lett.*, *34*, L02104, doi:10.1029/2006GL027953.

Tsurutani, B. T., and E. J. Smith (1974), Postmidnight chorus: A substorm phenomenon, *J. Geophys. Res.*, *79*, 118–127.

Tsurutani, B. T., O. P. Verkhoglyadova, G. S. Lakhina, and S. Yagitani (2009), Properties of dayside outer zone chorus during HILDCAA events: Loss of energetic electrons, *J. Geophys. Res.*, *114*, A03207, doi:10.1029/2008JA013353.

Vainio, R., et al. (2009), Dynamics of the Earth's particle radiation environment, *Space Sci. Rev.*, *147*, 187–231, doi:10.1007/s11214-009-9496-7.

Verkhoglyadova, O. P., B. T. Tsurutani, Y. Omura, and S. Yagitani (2009), Properties of dayside nonlinear rising tone chorus emissions at large L observed by GEOTAIL, *Earth Planets Space*, *61*, 625–628.

N. Cornilleau-Wehrlin, Station de Radioastronomie de Nançay, Observatoire de Paris, CNRS, F-18330 Nançay, France. (nicole.cornilleau@obs-nancay.fr)

P. M. E. Décreau and M. Parrot, LPC2E, CNRS, Orléans, France. (pdecreau@cnrs-orleans.fr; mparrot@cnrs-orleans.fr)

F. El-Lemdani Mazouz, Laboratoire Atmosphères, Milieux, Observations Spatiales, CNRS, 11 Boulevard D'Alembert, F-78280 Guyancourt, France. (farida.mazouz@latmos.ipsl.fr)

S. Grimald and A. Fazakerley, Mullard Space Science Laboratory, Holmbury St. Mary RH5 6NT, UK. (sg2@mssl.ucl.ac.uk; anf@mssl.ucl.ac.uk)

D. A. Gurnett and J. S. Pickett, Department of Physics and Astronomy, University of Iowa, Iowa City, IA 52242-1479, USA. (donald-gurnett@uiowa.edu; pickett@uiowa.edu)

N. P. Meredith, Physical Sciences Division, British Antarctic Survey, Natural Environment Research Council, Madingley Road, Cambridge CB3 0ET, UK. (nmer@bas.ac.uk)

O. Santolík, Department of Space Physics, Institute of Atmospheric Physics, Boční II 1401, 141 31 Praha 4, Czech Republic. (ondrej.santolik@mff.cuni.cz)

D. Schriver, Institute of Geophysics and Planetary Physics, University of California, Los Angeles, CA 90095-1567, USA. (dave@igpp.ucla.edu)